

Imazamox: A Quest for Polymorphic Modifications of a Chiral and Racemic Herbicide

Dario Braga,[†] Laura Chelazzi,[†] Fabrizia Grepioni,^{*,†} Saverio Nanna,[†] Katia Rubini,[†] Marco Curzi,[‡] Stefano Giaffreda,[‡] Heidi E. Saxell,[§] Matthias Bratz,[⊥] and Tiziana Chiodo^{*,||}

[†]Dipartimento di Chimica G. Ciamician, Università di Bologna, Via F. Selmi 2, Bologna, Italy

[‡]PolyCrystalLine, Via F. S. Fabri, 127/1, 40059 Medicina (BO), Italy

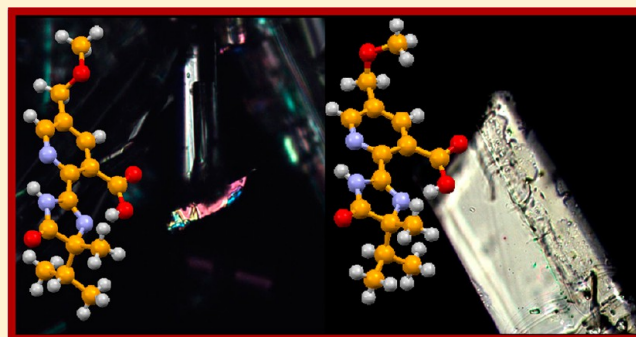
[§]Pulp Competence Centre, Stora Enso Oyj, Imatra Research Centre, FIN-55800, Imatra, Finland

[⊥]BASF (Formulation Development Fungicides), 67117 Limburgerhof, Germany

^{||}BASF (Crystalline Materials & Polymorphism), 67056 Ludwigshafen, Germany

Supporting Information

ABSTRACT: The structure–property relationships of new polymorphs of the chiral herbicide imazamox were investigated by X-ray diffraction, hot stage microscopy (HSM), and differential scanning calorimetry (DSC). Four different polymorphs of imazamox(R) were found. The relationship between different crystal forms, relative thermal stability, and possible conversions pathways was explored. Racemic imazamox, for which no polymorphic modifications could be observed, was also characterized in the solid state.



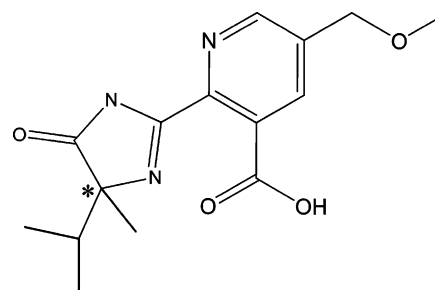
INTRODUCTION

Interest in the solid-state properties of drugs has blossomed in the last decades.¹ This interest is well deserved because an insufficient understanding of solid-state properties has led to serious setbacks over the years. Problems encountered range from the sudden unexpected inability to reliably produce a form that has been used in pivotal clinical studies to variations in the drug product properties due to seemingly random changes of the solid form during processes or storage. A thorough understanding of solid-state properties may create opportunities, benefitting both producers and the customers; for example, the production could be made more efficient and cheaper, and, more importantly, the properties of the drug or compounds could be improved.² In some cases, it may be possible to obtain patent protection for novel modifications with improved technical properties. In a crystallization process, the molecules arrange in an energetically favorable way, but it is not easy to understand the physical–chemical conditions that favor the formation of one form with respect to the others. The hydrogen bond interactions for neutral molecules and the reduction of void space compete for the best structural arrangement, but also external parameters (temperature, pressure, humidity rate, additives, etc.) have to be taken into account. The presence of one or more polymorphs may further complicate the crystallization process of compounds and represents a challenge for the industry. The current scientific literature reflects the importance of polymorphism in

pharmaceutical substances.¹ In agrochemicals, the basic interests are essentially the same, that is, investigating new forms, their properties, and their thermodynamical relationships; however, studies of polymorph screening of agrochemical compounds are still not so common as in the case of pharmaceutical compounds.³

Imazamox⁴ (Scheme 1) is an effective herbicide for the control of both terrestrial and aquatic vegetation. Imazamox is the common name for (±)-2-[4,5-dihydro-4-methyl-4-(1-methylethyl)-5-oxo-1H-midazol-2-yl]-5-(methoxymethyl)-3-pyridinecarboxylic acid and is a member of the imidazolinone

Scheme 1. Imazamox



Received: December 19, 2013

Revised: February 11, 2014

Table 1. Details of X-ray Data Measurements and Refinements

	imazamox(RS)			
	Form I	Form III	Form IV	imazamox(R)
formula	C ₁₅ H ₁₉ N ₃ O ₄	C ₁₅ H ₁₉ N ₃ O ₄	C ₁₅ H ₁₉ N ₃ O ₄	C ₁₅ H ₁₉ N ₃ O ₄
<i>M_r</i>	305.33	305.33	305.33	305.33
temp/K	103	293	293	103
$\lambda/\text{\AA}$	1.54178	0.71073	0.71073	1.54178
crystal system	orthorhombic	monoclinic	orthorhombic	orthorhombic
space group	<i>P</i> 2 ₁ 2 ₁ 2 ₁	<i>P</i> 2 ₁	<i>P</i> 2 ₁ 2 ₁ 2 ₁	<i>P</i> 2 ₁ 2 ₁ 2 ₁
<i>a</i> /\AA	7.2139(9)	7.262(2)	6.1344(4)	7.275(1)
<i>b</i> /\AA	14.934(2)	7.837(1)	12.3989(4)	16.048(3)
<i>c</i> /\AA	27.803(3)	27.115(2)	19.8456(7)	25.129(4)
β/deg		96.43(2)		
<i>V</i> /\AA ³	2995.4(6)	1533.5(5)	1509.5(1)	2934.0(8)
<i>Z</i>	8	4	4	8
<i>D_c</i> /Mg m ⁻³	1.354	1.322	1.344	1.383
μ/mm^{-1}	0.827	0.097	0.099	0.844
<i>F</i> (000)	1296.0	648.0	648.0	1296.0
2θ range/deg	6–116	3–44	3–54	6–114
reflns collected	3240	3784	2710	3731
indep reflns	2242	3398	2286	3313
<i>R</i> _{int}	0.061	0.022	0.030	0.044
refined params	406	414	190	406
<i>R</i> ₁ (obs)	0.058	0.047	0.043	0.039
<i>wR</i> ₂ (all)	0.136	0.105	0.055	0.091

class of herbicides, which also includes imazapic, imazapyr, imazethapyr, imazamethabenz, and imazaquin.⁴ All imidazolinone herbicides share a common mechanism of herbicidal action that involves the inhibition of acetolactate synthase (ALS). ALS is an enzyme found in plants and is required for the synthesis of essential branched chain amino acids as valine, leucine, and isoleucine, all of which are important for plant growth.⁵

In general, the herbicidal activity of the R-isomer is better than that of the racemic imidazolinone compounds. Chiral imidazolinone possessing the R configuration demonstrate about a 2-fold increase in herbicidal activity over the corresponding racemic mixture.⁴

In this work, we carried out a polymorph screening of imazamox(R) and imazamox(RS) using different solvents and additives in the crystallization medium to understand the physical–chemical conditions that can influence the formation of different polymorphs. All solid-state materials obtained were investigated by single crystal and powder X-ray diffraction, differential scanning calorimetry, variable temperature X-ray diffraction, and hot stage microscopy. A series of slurry experiments at room temperature and 50 °C and exposure to different humidity conditions were also conducted to ascertain the relative stability and possible conversion pathways of the crystal forms.

EXPERIMENTAL SECTION

Imazamox was provided by BASF S.p.A.; all other reagents were purchased from Sigma-Aldrich and used without further purification.

Crystallization from Solution. Imazamox(R) or imazamox(RS) (50 mg, 0.16 mmol) was dissolved in 4 mL of different solvents (acetonitrile, acetone, nitromethane, ethanol, 1-propanol, 1-butanol, diethyl ether, toluene, diisopropylether, *p*-xylene, hexane, dichloromethane, water, methanol, chloroform, THF, ethyl acetate, dioxane); the solutions were left to evaporate at room temperature, yielding single crystals or microcrystalline powders of different polymorphs of imazamox (see Table 2). Solutions prepared in the same way were

heated to 50 °C under stirring and left at 50 °C until complete evaporation, yielding single crystals or microcrystalline powders of different imazamox polymorphs (see Table 2). A third experiment concerned crystallization at room temperature with the addition of different inorganic salts (LiCl, 7 mg, 0.16 mmol, KCl, 11 mg, 0.15 mmol, CaCl₂, 9 mg, 0.08 mmol) to the imazamox solutions, with the goal of obtaining ionic co-crystals (see Table 3).⁶

Slurry Experiments. For the slurry experiments, imazamox(R) or imazamox(RS) (200 mg, 0.65 mmol) was suspended in different solvents (water, methanol, chloroform, ethyl acetate, THF, dioxane) in closed vessels and stirred either at room temperature or at 50 °C for three weeks. Polycrystalline powders were obtained in all cases.

X-ray Single Crystal Diffraction. X-ray data for form III and IV of imazamox(R) were collected at room temperature at the University of Bologna on an Oxford Diffraction X'Calibur diffractometer [Mo *K* α (λ = 0.71073 Å) radiation and graphite monochromator] equipped with a CCD detector (see Table 1 for data collection and refinement details). SHELX97⁷ was used for structure solution and refinement based on *F*². Non-hydrogen atoms were refined anisotropically. X-ray data for form I of imazamox(R) and imazamox(RS) were collected at BASF on a Bruker AXS, equipped with a CCD detector and a graphite monochromator, with Cu *K* α radiation. Absorption correction was performed with the SADABS software.¹⁰ Results of data collection and refinement are listed in Table 1. For all compounds, SHELX97⁷ was used for structure solution and refinement based on *F*². Non-hydrogen atoms were refined anisotropically. Hydrogen atoms were added in calculated positions. Mercury 2.3⁸ and CyLView⁹ were used for the graphical representation of the results.

X-ray Powder Diffraction. X-ray powder diffractograms in the 2θ range 5–50° (step size 0.01°, time/step 50 s, 40 kV × 40 mA) were collected on a Panalytical X'Pert PRO automated diffractometer equipped with an X'Celerator detector. Data were collected in Bragg–Brentano geometry, using Cu *K* α radiation without a monochromator. X-ray powder diffraction patterns simulated (Form I, III, IV) and observed (Form II) for the four polymorphic modifications of imazamox(R) are shown in Supporting Information, Figure S1.

Variable Temperature X-ray Diffraction. X-ray powder diffractograms of imazamox(R) and imazamox(RS) in the 2θ range 3–40° were collected on a Panalytical X'Pert PRO automated diffractometer equipped with an X'Celerator detector and an Anton

Table 2. Solvent Screening at RT and 50 °C for Imazamox(R)

solvent	RT	50 °C	solvent	RT	50 °C
water	I + III	I	ethanol	I	I
nitromethane	I	III	1-propanol	I	I
acetonitrile	I	I + III	1-butanol	I	I + III
methanol	I + III		diethyl ether	I	
acetone	I	I	toluene	I	
diisopropyl ether	I	I	dichloromethane	I	
chloroform	I + III	I	dioxane	I + III	
THF	I + III	I	<i>p</i> -xylene	I	
ethyl acetate	I + III		hexane	I	

Paar TTK 450 system for measurements at controlled temperature. The data were collected in open air in Bragg–Brentano geometry using Cu K α radiation without a monochromator.

Differential Scanning Calorimetry (DSC). DSC measurements were performed with a Perkin-Elmer Diamond. Samples (3–5 mg) were placed in a sealed aluminum pans. Heating was carried out at 5 °C min⁻¹ for all samples.

Thermogravimetric Analysis (TGA). TGA measurements were performed with a Perkin-Elmer TGA7 in the temperature range 40–350 °C under an N₂ gas flow, at a heating rate of 5 °C min⁻¹.

Hot Stage Microscopy (HSM). Hot stage microscopy measurements were carried out using a Linkam TMS94 device connected to a Linkam LTS350 platinum plate. Images were collected with the imaging software Cell, from a Visicam 5.0 stereoscope.

RESULTS AND DISCUSSION

Polymorph screening of imazamox chiral and racemic forms was carried out. For imazamox(R) four different polymorphs

Table 3. Solvent Screening at RT in the Presence of Alkaline and Alkaline Earth Salts

reagents	solvent	RT
imazamox(R)/KCl	water	I
imazamox(R)/KCl	ethanol	I
imazamox(R)/KCl	1-butanol	I
imazamox(R)/LiCl	water	IV
imazamox(R)/CaCl ₂	water ^a	III
imazamox(R)/CaCl ₂	water ^a	IV

^aForms III and IV were separately obtained in two distinct but analogous experiments.

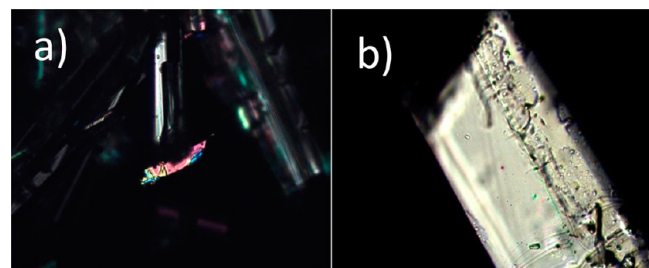


Figure 1. HSM images at RT of (a) Form I and (b) Form IV (both taken at 100 \times).

were found, named in order of characterization from Form I to Form IV, whereas for imazamox(RS) only one form was isolated. Relationships between crystalline forms were studied through a combination of solid state techniques, such as single crystal X-ray diffraction, X-ray powder diffraction at room and variable temperature, thermal analysis (DSC, TGA), and hot-stage microscopy (HSM).

Scheme 2. Slurry Experiments at RT and HT Starting from Form I

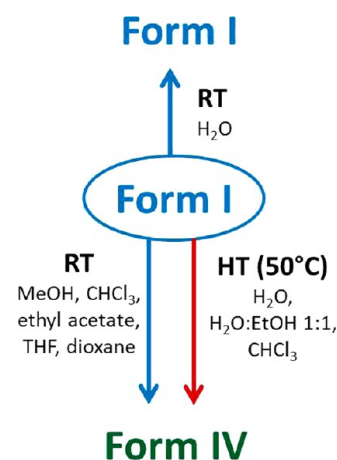
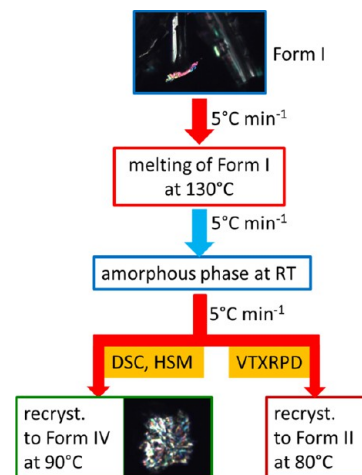


Table 4. Melting Points and Heat of Fusion of Imazamox(R) Polymorphs

	mp (°C)	ΔH_f (J g ⁻¹ , DSC data)
Form I	130(1) (DSC, peak)	41(1)
Form II	114(1) (DSC, peak)	30(1)
Form III	126(1) (HSM)	
Form IV	117(1) (DSC, peak)	102(1)

Scheme 3. Different Thermal Behavior of the Amorphous Phase, Obtained via Melting of Form I, Depending on the Technique Utilized (DSC and HSM vs. VTXPDP)



Imazamox(R). Solvent Screening. Form I corresponds to the sample as produced by BASE; solvent screenings at room

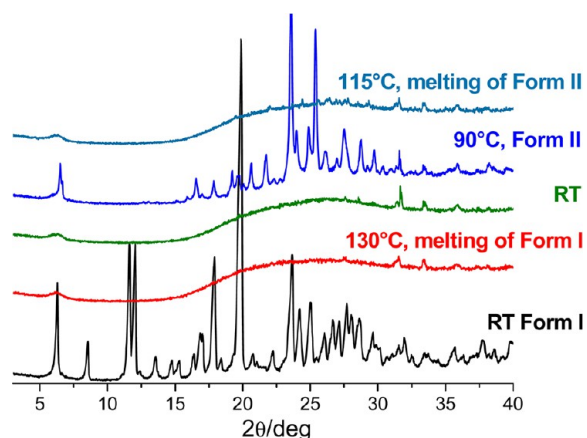
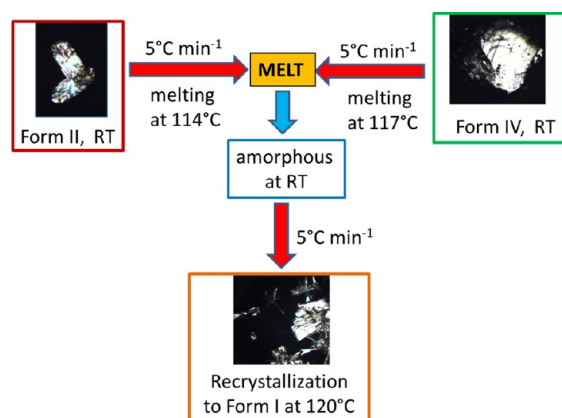


Figure 2. Variable temperature X-ray powder diffraction measurements on Form I. Heating and cooling processes are all conducted at $5\text{ }^{\circ}\text{C min}^{-1}$.

Scheme 4. Thermal Behavior of Form II and Form IV as Observed via DSC and HSM



temperature (RT) and high temperature (HT, $50\text{ }^{\circ}\text{C}$) were carried out (see Table 2). At room temperature, single crystals were always obtained, whereas solvent evaporation at $50\text{ }^{\circ}\text{C}$ invariably yielded microcrystalline powders. Recrystallization at RT from acetonitrile, acetone, nitromethane, ethanol, 1-propanol, 1-butanol, diethyl ether, toluene, diisopropylether, *p*-xylene, hexane, or dichloromethane always yielded crystals of Form I (Table 2). Recrystallization at room temperature from water, methanol, chloroform, THF, ethyl acetate, or dioxane yielded mixtures of Form I and Form III. Form III was obtained also by fast evaporation at $50\text{ }^{\circ}\text{C}$ from acetonitrile, 1-butanol, or nitromethane solutions (see Table 2). Form IV was obtained

via crystallization from an aqueous solution of LiCl or CaCl_2 (see Table 3), which was added to investigate the possibility of ionic co-crystals⁶ (ICCs) formation. Imazamox solubility is enhanced in these last solutions, and the increased ionic strength might have an effect on the nucleation and growth processes. In these crystallization conditions, a systematic improvement in crystals size and morphology was also observed (Figure 1).

Slurry Experiments. Slurry experiments were performed on Form I at room temperature (RT) and high temperature (HT, $50\text{ }^{\circ}\text{C}$). Slurry in methanol, chloroform, ethyl acetate, THF, or dioxane at RT and HT yielded Form IV as a microcrystalline powder, while slurry in water yielded Form I at RT and Form IV at HT (see Scheme 2). The temperature for HT experiments was chosen to simulate the stability tests commonly performed in the industry on agrochemical products.

The different results obtained on changing temperature conditions prompted us to investigate the thermal behavior and possible conversion properties of all forms, via VT-XRPD, TGA, DSC, and HSM measurements. Melting points are listed below in Table 4 (see Supporting Information Figures S2 and S3 for TGA and DSC traces, respectively).

Thermal behavior of Form I was investigated via both DSC and VT-XRPD. The two methods produce different results, as summarized in Scheme 3. VT-XRPD measurements (Figure 2) show that, after melting at ca. $130\text{ }^{\circ}\text{C}$, an amorphous phase is obtained on cooling; on a second heating cycle, recrystallization of this amorphous starts at ca. $80\text{ }^{\circ}\text{C}$ to a new polymorphic form that we named Form II; recrystallization is complete at $90\text{ }^{\circ}\text{C}$ (see Figure 2). The sample of Form II obtained via VT-XRPD was subsequently used for thermal behavior analysis (DSC and HSM).

DSC and HSM measurements on Form I replicate the behavior observed under the X-ray up to amorphous formation, but on a second heating cycle recrystallization is observed to a different polymorphic form, that is, to Form IV (see Scheme 3).

The different behavior in response to the technique utilized is not uncommon, as we have recently seen in ionic co-crystals of piracetam^{6d} and witnesses the necessity of combining optical, calorimetric, and diffraction techniques for a more comprehensive characterization of the thermal history of the sample under study.

Thermal behavior of Form II and Form IV is very similar: their melting points are extremely close (see Table 4), and cooling processes after the melting show, in both cases, recrystallization to Form I (DSC peak, see Scheme 4). It might be worth noting that Form II and Form IV, which melt at relatively low temperature, both recrystallize on cooling, while

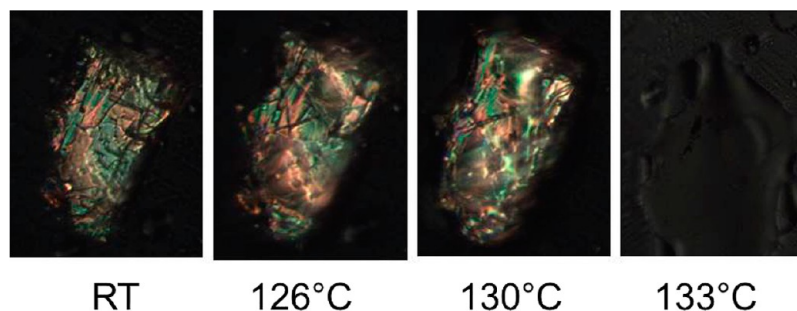


Figure 3. HSM on a single crystal of Form III, showing the melting process starting at ca. $126\text{ }^{\circ}\text{C}$ (heating rate $5\text{ }^{\circ}\text{C min}^{-1}$).

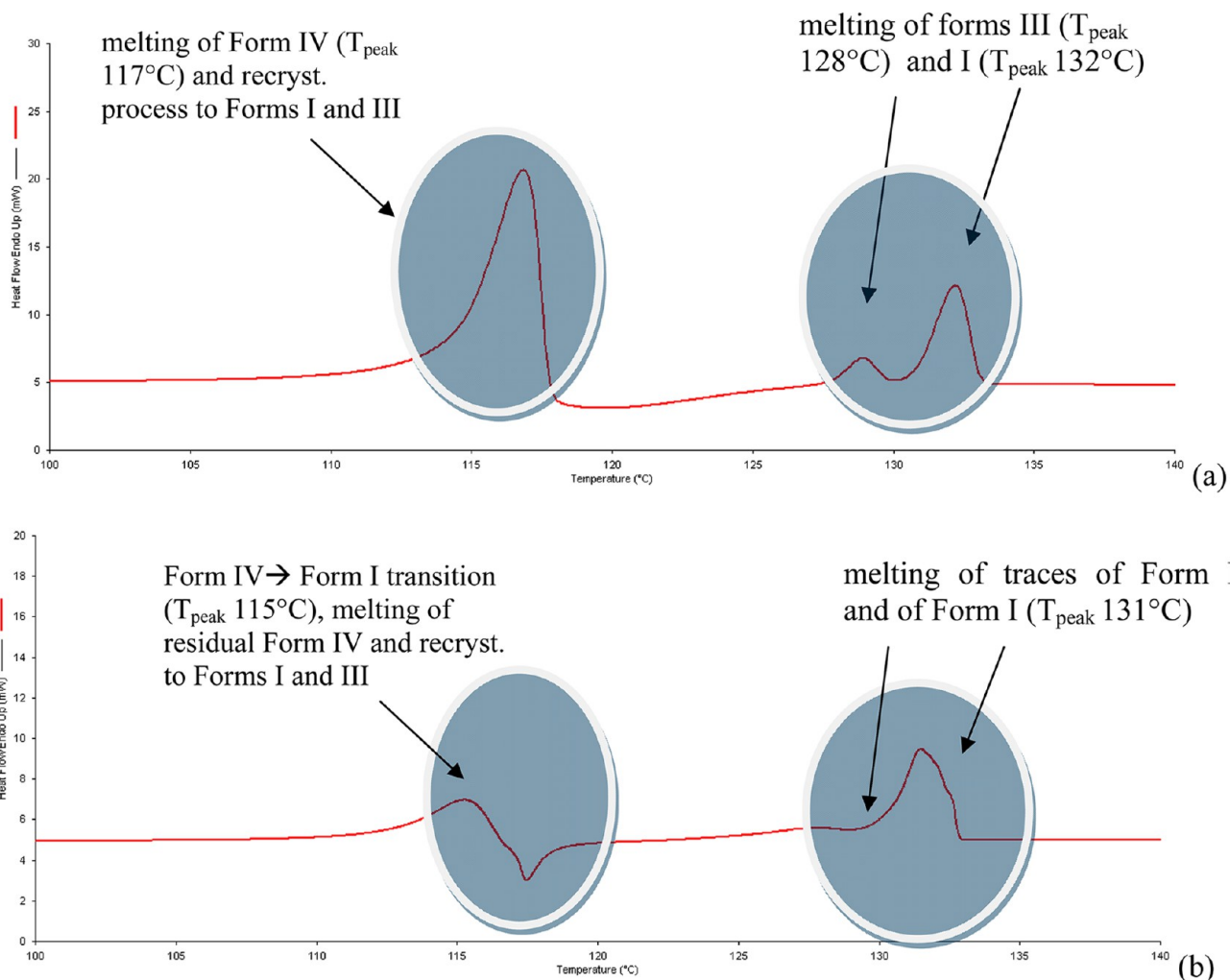


Figure 4. DSC traces for crystalline Form IV. Heating cycles conducted at (a) 5 °C min⁻¹ and (b) 1 °C min⁻¹.

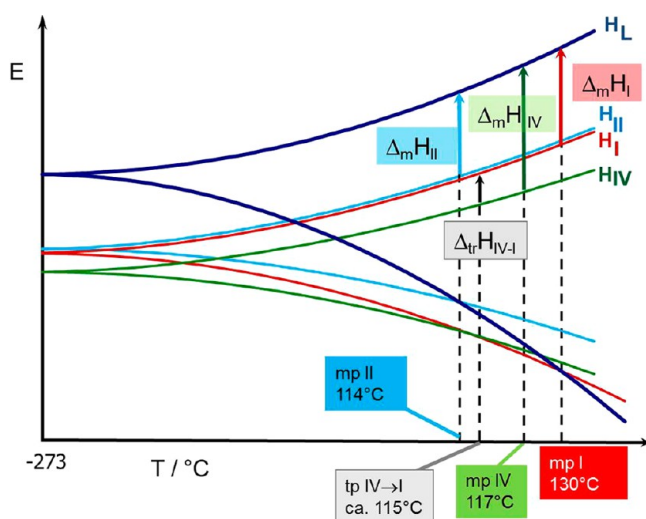


Figure 5. Qualitative $E-T$ plot (not on scale) for imazamox(R), showing the relationship between the different polymorphic modifications.

Form I, which melts at higher temperature, only forms amorphous phases upon cooling.

Imazamox(R) form III could be obtained only once in its pure form and as a limited amount of single crystals; for this

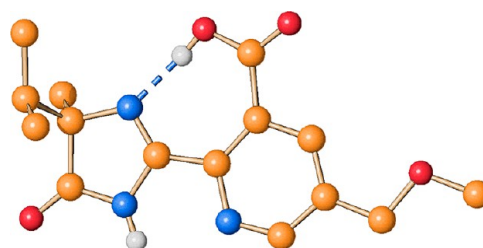


Figure 6. Intramolecular N...H-O interaction present in all imazamox(R) molecules (Form I is used here as an example).

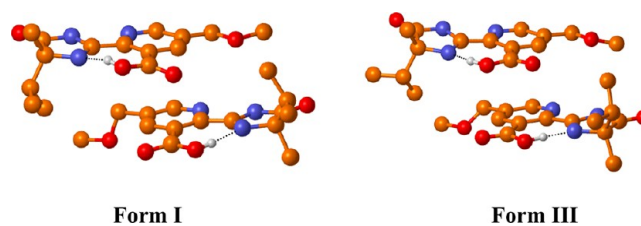


Figure 7. The dimers constituting the asymmetric units in Forms I and III. As the molecules in the two forms differ for the orientation of the isopropyl group, Form I and Form III can be considered conformational polymorphs.

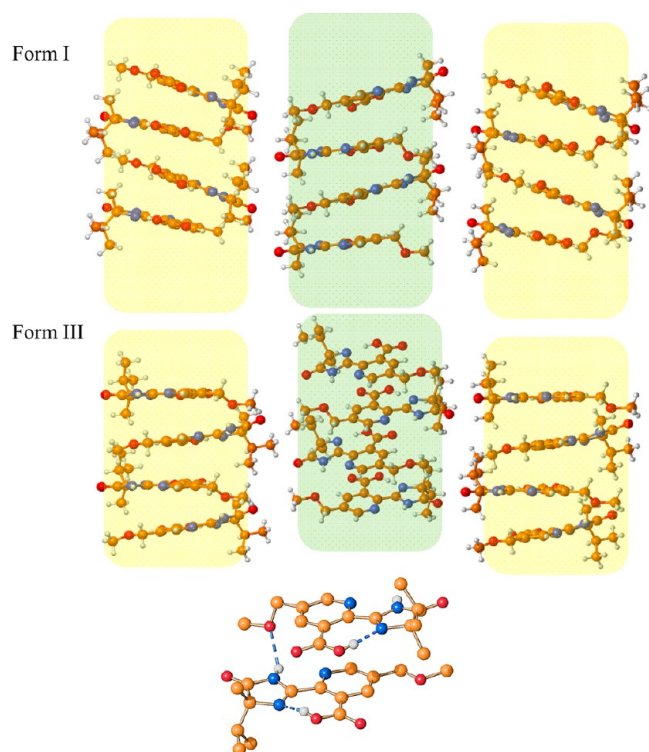


Figure 8. Different relative orientation of adjacent columns along the stacking direction in Form I (top) and Form III (middle). The intermolecular hydrogen bond along the pile, between the oxygen of the ether group on one molecule and the NH group on an adjacent molecule, is also shown (bottom) for Form I [$N(H)\cdots O$ 2.955(1) and 2.996(1) Å in Form I and Form III, respectively].

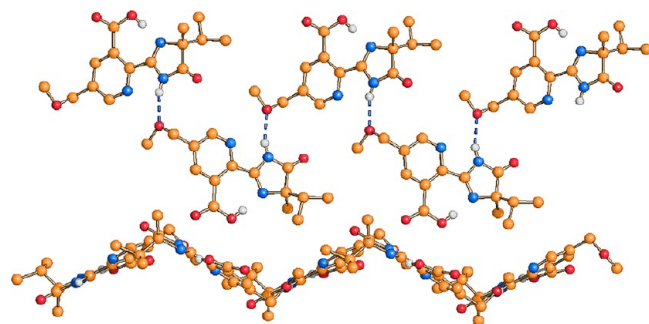


Figure 9. In Form IV, the dimer conformation is lost, and each molecule of imazamox is linked to other two molecules via hydrogen bonds, thus forming an infinite zigzag hydrogen bonded chain extending parallel to the b -axis direction. The chain is corrugated also if viewed laterally: the bottom part of the figure shows an adjacent chain in the crystal, running along the same direction but tilted by 90 deg.

reason, its thermal behavior was investigated only by HSM (Figure 3). No phase transition is observed for Form III before melting, which starts at ca. 126 °C and is complete at 133 °C (heating rate 5 °C min⁻¹).

Slurry experiments indicate that stability at room temperature is also dependent on the solvent employed, as Form I is maintained if water is used as a solvent; all other solvents yield form IV. At the same time, if we compare melting points and heat of fusion (see Table 4), it is easy to appreciate that Form I is characterized by a higher melting point and a lower heat of fusion.

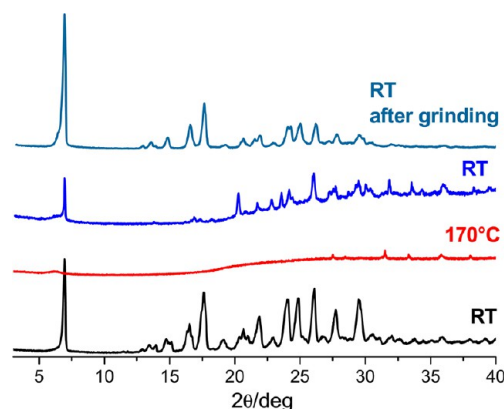


Figure 10. VT-XRPD measurements on imazamox(RS).

According to the Burger–Ramberger Rules, in particular to the heat-of-fusion rule, an enantiotropic relationship exists between Form I and Form IV: Form IV is the thermodynamically stable form at room temperature, while Form I is the thermodynamically stable form at high temperature. But how high is high? We were able to detect the transformation from Form IV to Form I only in a DSC measurement performed at a slow heating rate, that is, 1 °C/min (see Figure 4).

When Form IV is heated at 5 °C/min, melting is observed at 117 °C, followed by recrystallization to Forms I (major component) and III. At a slower heating rate, the melting cannot be completely avoided, but the most part of Form IV converts into Form I at ca. 115 °C, *that is, immediately before its melting point*, as it can be seen from the definitely lower ΔH of fusion. The molten portion recrystallizes, as observed in Figure 4a, into a mixture of Forms I and III (this last is present in lesser amount).

If we now combine all data collected via slurry and thermal characterization, we can try to draw a qualitative E – T diagram, which shows the relative stability of the four forms at different temperatures (see Figure 5). Figure 5b shows an expanded version of the most relevant part of the diagram; the diagram of course is not on scale, as melting points and the IV \rightarrow I phase transformation all occur in a narrow temperature range.

Structural Description. Crystal structures of Forms I, III, and IV were determined via single crystal X-ray diffraction. In the case of Form II, no single crystals could be grown, and its diffraction powder pattern, obtained in variable temperature XRPD measurements, was unfortunately never good enough to allow structural solution from powder.

The asymmetric unit in both Forms I and III of imazamox(R) is based on a pair of independent molecules arranged face-to face, while in Form IV only one molecule of imazamox is present. All three forms are characterized by the presence of an intramolecular hydrogen bond involving the carboxylic group and the nitrogen atom of the imidazoline ring [$N\cdots(H)O_{COOH}$ 2.520(1), 2.501(2), and 2.510(2) Å for Forms I, III, and IV, respectively] (see Figure 6).

Forms I and III show a similar packing arrangement and will be described together. The dimers constituting the asymmetric unit of both Forms I and III are shown in Figure 7: it can be seen that the two molecules within the dimers are arranged in space so that the two planar systems face each other, with an interplanar distance between the two six-membered rings of ca. 3.7 Å (Form I) and 3.9 Å (Form III). The main difference between the two forms is in the orientation of the isopropyl

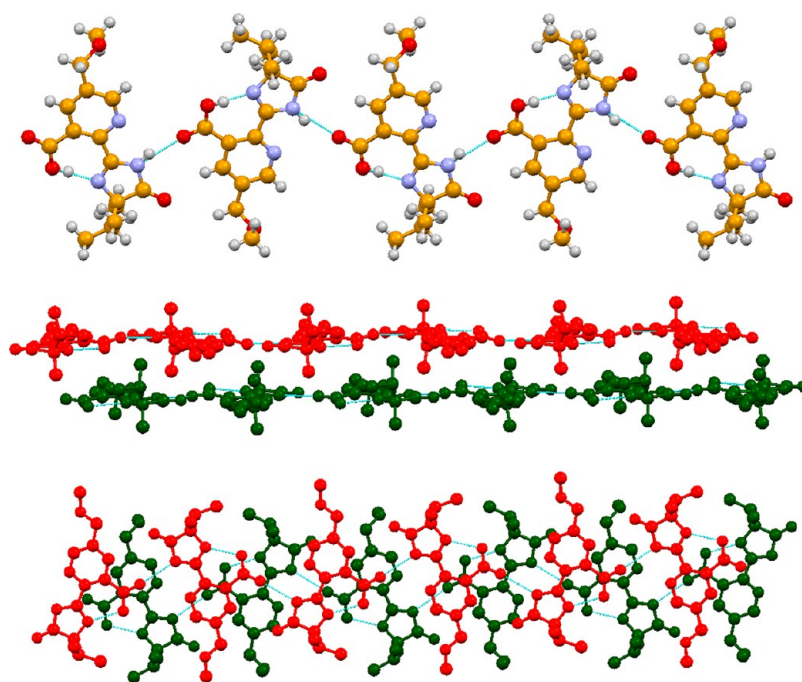


Figure 11. The infinite hydrogen bonded chain present in imazamox(RS), extending parallel to the crystallographic a -axis. Intermolecular hydrogen bonds are established between the N–H group on one imidazolone and the O_{CO} atom of the carboxylic group on an adjacent molecule [$N(H)\cdots O_{CO}$ 2.851(2) Å].

group. Forms I and Forms III can thus be considered conformational polymorphs.

The dimers of Figure 7 are both arranged in infinite stacks along the a -axis direction, but the relative orientation of adjacent columns along the stacking direction is different for the two polymorphs, as it can be seen from Figure 8. The similarities between the packing arrangements of Forms I and III are reflected in the similarity of their thermal behavior and melting point.

In crystalline Form IV, the dimeric pairing of molecules is not present, and the stacking motif is lost. In addition to the intramolecular hydrogen bond, each imazamox molecule is connected to two adjacent molecules via $N(H)\cdots O_{ether}$ ($N\cdots O$ distance 2.849(2) Å), thus forming an infinite zigzag hydrogen bonded chain extending parallel to the b -axis direction (see Figure 9). The chain is corrugated also if viewed laterally: the bottom part of the figure shows an adjacent chain in the crystal, running along the same direction but tilted by 90 deg.

Imazamox(RS). A solvent screening was also performed on imazamox(RS) both at room temperature (RT) and at high temperature (HT, 50 °C). Crystallization at RT from water, 1-propanol, diisopropylether, acetone, acetonitrile, THF, 1-butanol, and ethanol invariably yielded the starting material, that is, imazamox(RS). Slurry experiments on imazamox(RS) were also carried out at room temperature (RT) and at high temperature (HT, 50 °C). From these experiments, only microcrystalline powders of the starting form were obtained.

The thermal behavior of imazamox(RS) was investigated starting from VT-XRPD measurements. A polycrystalline sample of imazamox(RS), as provided by BASF, was shown to melt around 170 °C (see Figure 10); on cooling, recrystallization was observed (the process could be accelerated via grinding) to the starting form.

TGA and DSC measurements were also carried out; no phase transition was observed before melting, which occurs at

167 °C (peak temperature; see Supporting Information, Figure S4).

The results of an HSM analysis on a single crystal is in agreement with DSC and VT-XRPD observations, as the crystal melts completely at 165 °C.

In its crystals, racemic imazamox is characterized by an asymmetric unit containing two molecules of imazamox. The intramolecular hydrogen bond observed in chiral imazamox is obviously present also here, while the pattern of intermolecular hydrogen bonds is established here between the N–H group of imidazolone and the O_{CO} atom of the carboxylic group on an adjacent molecule. Infinite chains of imazamox(R) molecules are thus formed, which extend parallel to the crystallographic a -axis (see Figure 11).

CONCLUSION

Polymorph screening on chiral and racemic imazamox was performed. Four polymorphs of chiral imazamox were thermally characterized, and their structures were determined, except for Form II, which was obtained via variable temperature X-ray powder diffraction. Thermal relationships between all crystalline forms were studied, and the thermodynamically stable forms at room and high temperatures were identified. The addition of salts to crystallization media has shown potentialities in the nucleation step, allowing new polymorphic forms and improved crystal morphologies and sizes to be obtained. Potential polymorphs of agrochemical compounds, influenced by different experimental conditions, may prompt further investigation in the process of identifying stable forms during industrial manufacture. Solid-state study in the agrochemical field is still a forefront topic opened to new perspectives.

■ ASSOCIATED CONTENT

■ Supporting Information

TGA and DSC traces for imazamox(R) and imazamox(RS); crystallographic information files (CCDC 977677–977680) for all structures described herein. This material is available free of charge via the Internet at <http://pubs.acs.org>.

■ AUTHOR INFORMATION

Corresponding Authors

*(F.G.) e-mail: fabrizia.grepioni@unibo.it.

*(T.C.) e-mail: tiziana.chiodo@basf.com.

Notes

The authors declare no competing financial interest.

■ ACKNOWLEDGMENTS

Financial support by the University of Bologna, MIUR, and the Spinner2012 project (SV) is acknowledged.

■ REFERENCES

(1) (a) Bernstein, J. *Polymorphism in Molecular Crystals*; Oxford University Press: New York, 2002. (b) Brittain, H. G. *Polymorphism in Pharmaceutical Solids*; Marcel Dekker, Inc.: New York, USA, 1999. (c) Griesser, U. J. *Polymorphism in the Pharmaceutical Industry*; Hilfiker, R., Ed.; WILEY-VCH Verlag GmbH & Co. KGaA: Weinheim, Germany, 2006. (d) Braga, D.; Grepioni, F.; Chelazzi, L.; Campana, M.; Confortini, D.; Viscomi, G. C. The structure-property relationship of four crystal forms of rifaximin. *CrystEngComm* **2012**, *14*, 6404–6411.

(2) (a) McCrone, W. C. In *Physics and Chemistry of the Organic Solid State*; Fox, D., Labes, M. M., Weissberger, A. Eds.; Wiley Interscience: New York, 1965; Vol. 2, pp 726–767; (b) Halebian, J.; McCrone, W. *J. Pharm. Sci.* **1969**, *58*, 911–929. (c) Benghiat, V.; Leiserowitz, L. *J. Chem. Soc.* **1972**, *2*, 1763–1768. (d) Bernstein, J.; Davey, R. J.; Henck, J. V. *Angew. Chem.* **1999**, *38*, 3440–3461. (e) Almarsson, O.; Zaworotko, M. J. *Chem. Commun.* **2004**, 1889–1896. (f) Bulow, A. *Innovation Policy and the Economy* **4**; Jaffe, A. B., Lerner, J., Stern, S., Eds.; The MIT Press: Cambridge, 2004; pp 145–185; (g) Vishweshwar, P.; McMahon, J. A.; Bis, J. A.; Zaworotko, M. J. *J. Pharm. Sci.* **2006**, *95*, 499–516. (h) Blagden, N.; de Matas, M.; Gavan, P. T.; York, P. *Adv. Drug Delivery Rev.* **2007**, *59*, 617–630. (i) Bernstein, J. *Cryst. Growth Des.* **2011**, *11*, 632–650.

(3) (a) Griesser, U. J.; Weigand, D.; Rollinger, J. M.; Haddow, M.; Gstrein, E. *J. Therm. Anal. Calorim.* **2004**, *77*, 511–522. (b) Chopra, D.; Mohan, T. P.; Sundaraja Rao, K.; Guru Row, T. N. *CrystEngComm* **2005**, *7*, 374–379. (c) Nauha, E.; Saxell, H.; Nissinen, M.; Kolehmainen, E.; Schäfer, A.; Schlecker, R. *CrystEngComm* **2009**, *11*, 2536–2547. (d) Nauha, E.; Ojala, A.; Nissen, M.; Saxell, H. *CrystEngComm* **2011**, *13*, 4956–4964.

(4) (a) Doehner Jr., R. F.; Lodner, D. W.; Finn, J. M. U. S. Patent, 5.334.576, 1994; (b) Wepplo, P. J.; Drabb, T. W. U. S. Patent, US2002/007753A1, 2004.

(5) Tan, S.; Evans, R. R.; Dahmer, M. L.; Singh, B. K.; Shaner, D. L. Imidazolinone-tolerant crops: history, current status and future. *Pest Manage. Sci.* **2005**, *61*, 246–257.

(6) (a) Braga, D.; Grepioni, F.; Maini, L.; Prosperi, S.; Gobetto, R.; Chierotti, M. R. *Chem. Commun.* **2010**, *46*, 7715–7717. (b) Braga, D.; Grepioni, F.; Lampronti, G. I.; Maini, L.; Turrina, A. *Cryst. Growth Des.* **2011**, *11*, 5621–5627. (c) Braga, D.; Grepioni, F.; Maini, L.; Lampronti, G. I.; Capucci, D.; Cuocci, C. *CrystEngComm* **2012**, *14*, 3521–3527. (d) Braga, D.; Grepioni, F.; Maini, L.; Capucci, D.; Nanna, S.; Wouters, J.; Aerts, L.; Quéré, L. *Chem. Commun.* **2012**, *48*, 8219–8221.

(7) Sheldrick, G. M. *SHELXL97: Program for Crystal Structure Determination*; University of Göttingen: Germany, 1997.

(8) Macrae, C. F.; Bruno, I. J.; Chisholm, J. A.; Edgington, P. R.; McCabe, P.; Pidcock, E.; Rodriguez-Monge, L.; Taylor, R.; van de

Streek, J.; Wood, P. A. MERCURY 3.0: New Features for the Visualization and Investigation of Crystal Structures. *J. Appl. Crystallogr.* **2008**, *41*, 466–470.

(9) Legault, C. Y. *CYLview*, v 1.0b; Université de Sherbrooke: Canada, 2009.

(10) SADABS; Bruker AXS Inc.: Madison, Wisconsin, USA, 2001.